Taylor & Francis
Taylor & Francis Group

Check for updates

The effect of undulations on the particle stress in dilute suspensions of rod-like particles

Mohsen Daghooghi and Iman Borazjani ◉

Department of Mechanical and Aerospace Engineering, University at Buffalo, The State University of New York, Buffalo, NY, USA

ABSTRACT

We compared a dilute suspension of undulating rod-like particles (active suspension) with a similar one consisting of rigid rods (passive suspension) under shear flow. For the active suspension, a synchronised group of swimmers propel themselves forward by passing a travelling wave through their bodies while at the same time rotate due to planar background shear flow. Using a high resolution immersed body numerical simulations, we have shown that an active particle can exhibit complex dynamics, which is fundamentally different from a similar passive one. The orientation of the active particle consists of two separate oscillations: a low-frequency oscillation similar to the passive particle (determined by shear rate) and a high-frequency oscillation due to the body undulations. Nevertheless, different dynamics did not result in a major difference in rheological behaviour of the suspension. We found that the effective viscosity of the active suspension is equal to that of a passive one, i.e. self-propulsion did not change the viscosity of the suspension probably because of the high shear rate and inertia of our simulations.

1. Introduction

A suspension of self-propelled particles, which is categorised under active suspensions, has been the subject of many recent experimental and theoretical investigations (Elgeti, Winkler, & Gompper, 2015; Saintillan & Shelley, 2015) due to numerous applications (Ozin, Manners, Fournier-Bidoz, & Arsenault, 2005), including drug delivery in medicine (Balasubramanian et al., 2011). Such particles can exhibit interaction mechanisms that favour velocity alignment of neighbouring particles, often display collective behaviours like swarming (Yang, Marceau, & Gompper, 2010) and flocking (collective, coherent motion of large numbers of self-propelled particles) (Toner, Tu, & Ramaswamy, 2005). Examples of such behaviour range from micro-scale (sperm, bacteria, nano-rods – see Lauga & Powers, 2009 for review) to macro-scale (fish Daghooghi & Borazjani, 2015; Gazzola, Tchieu, Alexeev, de Brauer, & Koumoutsakos, 2016, robots

---

CONTACT Iman Borazjani ✉ iman@buffalo.edu

Becker, Masoud, Newbolt, Shelley, & Ristroph, 2015; Daghooghi & Borazjani, 2016). Over the past decade, a number of different realisations of active particles have been proposed based on anisotropic rod-like shapes (Saintillan & Shelley, 2007; Wensink, 2012) as a special class of biological systems (Yang et al., 2010).

Organisms have developed a variety of different mechanisms for propulsion such as using flagella, cilia or surface waves (Lauga & Powers, 2009). Propagating a travelling wave through the body is a common mechanism to generate propulsion in a wide range of small aquatic organisms from planktons (Brennen & Winet, 1977) to fish larvae (Li, Müller, van Leeuwen, & Liu, 2012). This mechanism produces thrust and pushes microorganisms forward in the absence of shear. However, when a shear is imposed in the surrounding fluid, the microorganism also experience a viscous torque due to the shear. Therefore, the orientation of the swimmer is determined by both the viscous torque and force production due to body undulation.

In addition to the dynamics that these suspensions exhibit, their rheology is also of interest. In fact, self-propulsion is known to play a drastic role in changing the rheological behaviour of active suspensions. Assuming pure relaxational dynamics, Hatwalne, Ramaswamy, Rao, and Simha (2004) was the first to consider the effects of self-propulsion on the viscosity of active suspensions. The viscosity reduction for dilute suspensions has been addressed in some theoretical studies (Gyrya, Lipnikov, Aranson, & Berlyand, 2011; Haines, Sokolov, Aranson, Berlyand, & Karpeev, 2009) indicating that the shear viscosity in a dilute suspension of swimmers can be smaller than the viscosity of the ambient liquid. Based on the proposed theory, the necessary condition for viscosity reduction in planar shear flow is the particle's tumbling (Haines et al., 2009). However, experimental observations on the effective viscosity of dilute suspensions of swimming aerobic bacterium show significant reduction in the viscosity without noticeable tumbling compared to that of the same suspension of nonmotile bacteria (Sokolov, Aranson, Kessler, & Goldstein, 2007; Sokolov & Aranson, 2009).

In this paper, we use numerical simulations to investigate aspects of orientation dynamics in suspensions of self-locomoting rods at low (but not negligible) Reynolds numbers. The purpose of this research is to study the role of body motion (self-propulsion) on the dynamics and rheological behaviour of a dilute suspension, where particles interact only with the background flow and not with each other. We model the swimmer as a flexible (active) rod with an aspect ratio of Length/Diameter $=$ 25 and compare it with an identical rigid (passive) rod under the same flow conditions. To reduce computational costs, we consider a single swimmer in a computational domain and implement periodic boundary conditions to create a dilute suspension of particles.

2. Method and material

The numerical method used to simulate the motion of neutrally buoyant rod in the shear flow is the curvilinear immersed boundary (CURVIB) method (Asgharzadeh & Borazjani, 2016; Borazjani, Ge, & Sotiropoulos, 2008; Ge & Sotiropoulos, 2007; Gilmanov & Sotiropoulos, 2005) coupled with the dynamics of a moving object. We have used the quaternion-angular velocity equations, instead of the conventional rotation matrix, to find the instantaneous orientation of the particle in order to avoid numerical drift. These solvers are coupled together through a strong-coupling fluid-structure interaction (FSI) approach (Borazjani et al., 2008). This computational set-up is an extension to our previous framework (Daghooghi and Borazjani 2015), which was used to simulate the motion of a rigid (passive) ellipsoid in shear flow. Therefore, we briefly discuss the method and the kinematics of the active particle below.

2.1. Numerical framework: structure/flow solvers and 3D rigid body rotation

In this work, the motion of the active particle is a combination of an undulatory motion (prescribed with respect to a moving coordinate system), and a rotation/translational one (calculated through FSI). The undulatory motion is a backward travelling wave (Figure 1(a)), which is observed in experimental observations and measurements for fish larvae (Li et al., 2012). The following equation describes the lateral undulations of the active particle:

$$h(s,t) = a(s) \sin\left(\frac{2\pi}{\lambda}s - \mathfrak{w}t\right) \tag{1}$$

where s is the dimensionless distance from the head along the longitudinal axis of the particle ($0 < s < 1$); $h(s,t)$ is the lateral excursion at dimensionless time t; $a(s)$ is the dimensionless amplitude envelope function; λ is the length of the body wave; $\mathfrak{w}$ is the angular frequency– see Figure 1(a). All variables are non-dimensionalised by a characteristic length L (stretched length of the object) and a characteristic velocity $U = a_{\max}(2\pi f)L$, where f is the frequency of the undulations and $a_{\max} = a(1) = .1$ is the maximum amplitude of the lateral undulations. This is the maximum lateral velocity due to undulations, which occurs at the anterior part ($s = 1.0$) of the particle. Based on selected characteristic length and velocity, we set (Daghooghi and Borazjani 2016):

$$a(s) = a_{\max}e^{2.18(s-1)} \quad \lambda = 0.65 \quad \mathfrak{w} = 10 \tag{2}$$

The body undulation along with the bulk shear flow create velocity and pressure fields around the particle and exert a hydrodynamic force/torque on its surface. The exerted hydrodynamic force/torque make the particle to translate and rotate. The angular and translational momentum can be obtained by integrating hydrodynamic force/torque through a strong coupling (iteratively) FSI (Daghooghi & Borazjani, 2015) as:
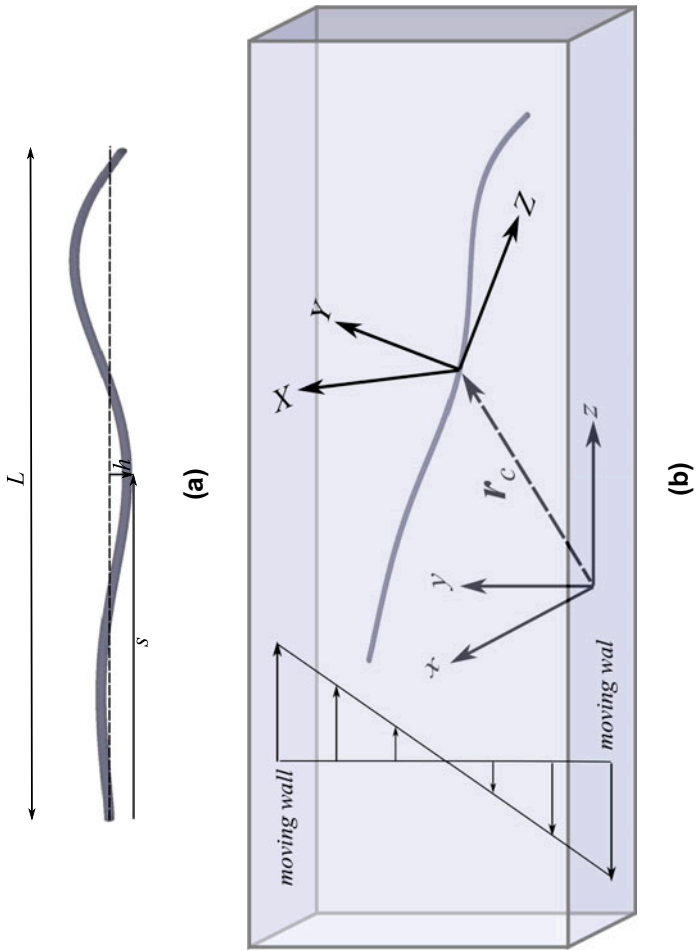
Figure 1. (a) The undulatory motion is prescribed with respect to the non-inertial frame of reference is a backward travelling. (b) The non-inertial frame of reference is attached to the particle's centre of mass.

$$\mathcal{M}\frac{\mathrm{d}^2\mathbf{r}_c(t)}{\mathrm{d}t} = \mathbf{F}(t) \tag{3}$$

$$\frac{\mathrm{d}\mathbf{L}(t)}{\mathrm{d}t} = \mathbf{M}(t) \tag{4}$$

where $\mathbf{r}_c(t)$ is the position vector of the particle's centre of mass (COM) with respect to the inertial frame of reference (Figure 1(b)), $\mathbf{F}(t)$ and $\mathbf{M}(t)$ denote the total hydrodynamic force and torque exerted on the surface of the body, respectively, $\mathcal{M}$ is dimensionless mass of particle and $\mathbf{L}$ is the angular momentum of the body defined as:

$$\mathbf{L}(t) = \left[\mathbb{R}(t)\mathbb{I}_b\mathbb{R}^T(t)\right]\mathbf{\Omega}(t) \tag{5}$$

where $\mathbf{\Omega}$ is angular velocity vector, $\mathbb{R}$ is the rotation matrix and $\mathbb{I}_b$ is the moment of inertia calculated with respect to the moving coordinate system (attached to the body) (Daghooghi & Borazjani, 2015). The moving coordinate system is attached to the particle's COM and a schematic illustrations of moving and inertial frames are shown in Figure 1(b). Instead of the conventional way of solving for the time evolution of the rotation matrix, it is preferred to use quaternions, $\mathbf{q}(t)$, to represent the orientation of the body in three-dimensional space (Baraff, 2001) to avoid the numerical drift. The quaternion vector at each specific time instant can be calculated by solving the following equation:

$$\frac{\mathrm{d}\mathbf{q}}{\mathrm{d}t} = \frac{1}{2}\mathbf{q} \times \mathbf{\Omega} = \frac{1}{2}\begin{bmatrix} 0 & -\Omega_1 & -\Omega_2 & -\Omega_3 \\ \Omega_1 & 0 & -\Omega_3 & \Omega_2 \\ \Omega_2 & \Omega_3 & 0 & -\Omega_1 \\ \Omega_3 & -\Omega_2 & \Omega_1 & 0 \end{bmatrix}\begin{bmatrix} q_1 \\ q_2 \\ q_3 \\ q_4 \end{bmatrix} \tag{6}$$

Since we still need the rotation matrix to calculate the instantaneous moment of inertia in Equation (5), $\mathbb{R}(t)$ will be computed as an auxiliary variable from $\mathbf{q}(t)$ as the following:

$$\mathbb{R} = \begin{bmatrix} 1 - 2q_2^2 - 2q_3^2 & 2(q_1q_2 - q_0q_3) & 2(q_1q_3 + q_0q_2) \\ 2(q_1q_2 + q_0q_3) & 1 - 2q_1^2 - 2q_3^2 & 2(q_2q_3 - q_0q_1) \\ 2(q_1q_3 - q_0q_2) & 2(q_2q_3 + q_0q_1) & 1 - 2q_1^2 - 2q_2^2 \end{bmatrix} \tag{7}$$

Now we have enough equations (Equations (3)–(7)) to close the system of equations and solve for all unknown variables of the particle dynamics $\left(\mathbf{r}_c, \mathbf{L}, \mathbf{\Omega}, \mathbb{R}, \mathbf{q}\right)$. Finally, the position vector on the surface of swimmer is calculated as:

$$\mathbf{r}(t) = \mathbb{R}(t)\left[\mathfrak{R}(t) - \mathbf{r}_c(0)\right] + \mathbf{r}_c(t) \tag{8}$$

where $\mathfrak{R}$ is position vector of a material point on the surface of swimmer with respect to the body-frame coordinate system (attached to the body), and $\mathbf{r}_c(0)$ is the initial vector position of the COM, which is also the origin of the body-frame coordinate system.

The equations governing the motion of an incompressible Newtonian viscous fluid are the unsteady 3D Navier–Stokes equations. Governing equations are solved over high-resolution grids using a hybrid staggered/non-staggered discretisation with QUICK scheme for the convective and central difference for the viscous terms. The equations are integrated in time using an efficient, second-order accurate fractional step methodology with a Newton–Krylov solver for the momentum equations, and a GMRES solver enhanced with multi-grid as a pre-conditioner for the Poisson equation (Borazjani et al., 2008; Ge & Sotiropoulos, 2007). The code is parallelised using MPI and the parallel libraries of PETSc (Balay et al., 2001) to efficiently utilise the supercomputing facilities available to the authors. To handle the moving boundaries, a sharp-interface immersed boundary method is used (Borazjani et al., 2008; Ge & Sotiropoulos, 2007; Gilmanov & Sotiropoulos, 2005). The sharp-interface is maintained by reconstructing the boundary conditions (no slip) at the nodes that are exterior to, but adjacent to the immersed-boundary surface using interpolation along the local normal to the boundary, which is shown to be second-order accurate (Gilmanov & Sotiropoulos, 2005). Using the strong-coupling partitioned approach with under-relaxation (Borazjani et al., 2008), the fluid and particle domains are separately advanced in time, but the simultaneous (implicit) solution of both equations is achieved through fluid/structure sub-iterations (Daghooghi & Borazjani, 2015). The method has been applied to a variety of complex flow problems such as rheology (Daghooghi & Borazjani, 2015), aquatic swimming (Daghooghi & Borazjani, 2015, 2016) and cardiovascular flows (Asgharzadeh & Borazjani, 2016).

2.2. Formulation of rheological parameters

After calculating the kinematics of the particle due to exerted hydrodynamical force/torque, the stress tensor of the suspension can be obtained as (Batchelor 1970):

$$\Sigma_{ij} = -\delta_{ij}\frac{1}{V}\int_{V_f} p\,\mathrm{d}V + \mu\left(\frac{\partial \mathcal{U}_i}{\partial x_j} + \frac{\partial \mathcal{U}_j}{\partial x_i}\right) + \Sigma_{ij}^p \tag{9}$$

where p is the pressure, V and V_f are the total volume of suspension and the volume occupied by the fluid, respectively, and $\frac{\partial \mathcal{U}_i}{\partial x_j}$ is the volume averaged velocity gradient. Σ_{ij}^p represents the contribution to the bulk stress due to the presence of particles and referred to as 'particle stress'. The non-dimensional form of this contribution (dividing particle stress by ρU^2) reads as (Batchelor 1970):

$$\Sigma_{ij}^p = \frac{1}{V}\sum_{n=1}^{N}\int_{(A_p)_n} [x_j\sigma_{ik}n_k - Re^{-1}(u_in_j + u_jn_i)]\mathrm{d}A$$
$$- \frac{1}{V}\sum_{n=1}^{N}\int_{(V_p)_n} \rho x_j a_i \mathrm{d}V$$

$$-\frac{1}{V}\int_V \rho u_i' u_j' \mathrm{d}V \tag{10}$$

where $Re = (UL)/\nu$ is the Reynolds number based on the swimmer's characteristic length and velocity, V_p is the particle's volume, N is the total number of particles in the suspension, σ_{ik} is the Newtonian stress, u_i' are velocity fluctuations, x_i is the displacement vector measured from the COM and a_i is the particle acceleration calculated at **r**. Finally, the relative viscosity is defined by:

$$\eta_r = 1 + \frac{Re}{\dot{\gamma}}\mathrm{Sym}(\overline{\Sigma_{yz}^p}) \tag{11}$$

where $\dot{\gamma}$ is dimensionless shear rate (shear rate divided by $U/L = .2\pi f$, where f is the frequency of the rod's undulations), $\mathrm{Sym}(\bullet)$ denotes the symmetric part of $\bullet$, $\overline{\bullet}$ is the averaged value of $\bullet$ over rotational timescale, and (x, y, z) are corresponding to vorticity, flow, and velocity gradient directions, respectively, as shown in Figure 1. It should be noted that in Stokesinan dynamics, in which suspended particles are both force-free and torque-free, only the first term on the right-hand side of Equation (10) (stresslet) should be considered. Two other terms of Equation (10) extend this framework to non-zero Reynolds numbers (Batchelor, 1970). This formulation has been successfully applied to study inertial effects in suspensions of particles with various shapes (Aidun & Clausen, 2010; Daghooghi & Borazjani, 2015; Haddadi & Morris, 2014).

2.3. Computational set-up

The computational set-up is similar to the one used in our previous work (Daghooghi & Borazjani, 2015). The flow is initialised with a linear shear flow with the dimensionless shear rate $\dot{\gamma} = 1.0$. The shear rate is chosen such that the timescales of the background shear flow and undulations are approximately equal. Such shear rates make the induced velocity due to shear velocity comparable to velocity of the undulations. In fact, the maximum shear velocity is .75 times of the maximum lateral velocity due to undulations. Boundary conditions in the velocity gradient direction (y-direction in Figure 1) are moving walls in opposite directions, and other directions are set to be periodic (Daghooghi & Borazjani, 2014). The implementation of periodic boundary conditions creates a planer array of particles that rotate in-phase, i.e. a periodic suspension. Such simulations can be a good approximation of a homogenous suspension in low concentrations in which particles are sufficiently far from each other and close-distance interactions are less likely to happen (Daghooghi & Borazjani, 2015). A schematic of the computational domain is depicted in Figure 1.

In both cases (active and passive) investigated in this paper, volume fraction and Reynolds number are fixed at $\phi = .001$ and $Re = 1.0$. These values of volume fraction and Reynolds number are in agreement with the assumption of dilute suspension under influence of inertia. Simulations start by placing the

COM of the particle (active and passive) in the centre of computational domain such that body attached and inertial reference frames coincide. In other words, the passive particle is aligned in the flow direction and the active swimmer start undulating in the $x - z$ plane. Simulations of passive particles under inertial effects have shown that the final state of rotational mode for prolate spheroids (rods) and moderate amount of inertia is tumbling (Rosén, Do-Quang, Aidun, & Lundell, 2015), as we picked for our passive particle. For the active particle at this initial orientation, undulations could be either in $x - z$ or $y - z$ planes. The former case is chosen, as it creates a more complicated flow pattern (flow rotation due to shear and undulation are perpendicular), compared to the latter one (flow rotation due to shear and undulation are in the same plane).

The computational domain is $.5\,\mathrm{L} \times 1.5\,\mathrm{L} \times 1.5\,\mathrm{L}$ along x, y, and z directions, respectively, and discretised uniformly with a grid size selected as $\Delta = .01\,\mathrm{L}$. This grid size has opted based on the grid sensitivity tests for various spherical and ellipsoidal particles at similar Reynolds numbers (Daghooghi & Borazjani, 2015). Computational time step is .01 for the passive particle, and for .0026 for the active particle (smaller time step for active suspension is due to the stability of FSI).

3. Results and discussion

3.1. Flow visualisation and kinematics of the particle

As a particle is released in a shear flow, it starts to rotate due to the vorticity of the bulk flow. However, the active particle creates another vorticity vector, which is initially perpendicular to the shear flow vorticity and superposition of these two vorticity vectors creates a complex flow. In Figure 2, the out-of-plane vorticity contours around the rod are visualised in two perpendicular planes when both particles have rotated $\theta = .1$ radians around x-direction. In the left side of the figure, vorticity along the x-direction is shown for simulations of passive (upper part) and active (lower part) particles. We coloured $\omega_x = 1.0$ (equal to the vorticity of undisturbed flow) as white, regions coloured as red and blue rotate with higher and lower angular velocity with respect to the undisturbed (bulk) flow, respectively. Comparing upper and lower left figures, there are general similarities between this component of vorticity for both particles. Fluid particles rotates faster at both ends of rods with symmetric relative vorticity (vorticity with respect to the bulk flow). Highest values of vorticity at both ends is due to the fact that at these points rod has the highest value of velocity and fluid particles attached to these points experience high value of rotation. There are also some differences such as the break up of higher vorticity (red) in the rear and lower vorticity (blue) in the middle of the active rod. Moreover, the undulatory rod (lower left figure) has a higher relative vorticity compared to the rigid rod, which is probably due to higher tip velocity caused by body undulations, i.e. at the

shown time instant the lower vorticity region are larger at the ends of the active rod.

In the right side of Figure 2, out-of-plane vorticity is shown in the mid-plane that passes through the body and perpendicular to the previous plane ($X - Z$ plane in Figure 1(b)). In fact, this plane rotates with the body around the x-axis itself. For an undulatory rod, as clearly shown in the lower right figure, an array of vortices with alternating normal directions is formed due to the body rotation. Sign and strength of these vortices change during the time as the travelling wave passes through the body. Theoretical analysis (the body velocity and fluid velocity should match at the body surface, i.e. no-slip condition) and experimental measurements (Willert & Gharib, 1991) of the surrounding fluid revealed that the sign (shown as red or blue in this figure) and magnitude of fluid rotation close to the body surface is correlated to the body kinematics. Consequently, the vorticity of fluid near the body surface is equal to the angular velocity of the body surface itself. These vortices are stronger than the vorticity in the perpendicular plane (lower left figure), which are caused by the shear flow. On the other hand, normal vorticity for the rigid rod in the similar plane (upper right figure) is significantly weaker in the absence of body movements.

As stated earlier, we expect rich kinematics for the active particle as the consequence of combination of a shear flow and the body motion. Figure 3 shows three components of angular velocity of active and passive particles as a function of time. Note that for ω_x (Figure 3(a)) a whole cycle is shown, whereas for two other components (Figure 3(b) and 3(c)) only a half cycle is shown as they are symmetric for the other half. The most evident point about the angular velocity vector is that passive particle has a very low frequency of oscillation due to its rotation (tumbling), whereas components of this vector consists of two frequencies for the active particle, a low-frequency oscillation similar to the passive particle and a high-frequency oscillation due to the body undulations. In fact, the kinematics of the active particle is determined by two important physical timescales: the angular velocity of body undulations w and the shear rate imposed to the suspension $\dot{\gamma}$. Frequencies of oscillations in Figure 3 are controlled by these timescales.

The angular velocity about the vorticity direction ω_x (shown in Figure 3(a)) for both particles have two maxima, for which the projected area against the flow is maximum as well. The first maximum of angular velocity in active and passive rods overlap but the second one is shifted because the active particle is swimming when it is aligned with the flow and make the rotation time slightly longer (see the period of rotation T in Table 1). The maximum of ω_x is very close to one for the passive rigid rod, which is in agreement with analytical/numerical solutions for high aspect ratio spheroids (Daghooghi & Borazjani, 2015; Jeffery, 1922). For the active particle, ω_x is very similar to the passive one, but it oscillates (with a frequency equal to that of body undulations) around ω_x of the rigid rod with an amplitude that changes dynamically during the cycle of rotation. Nevertheless,
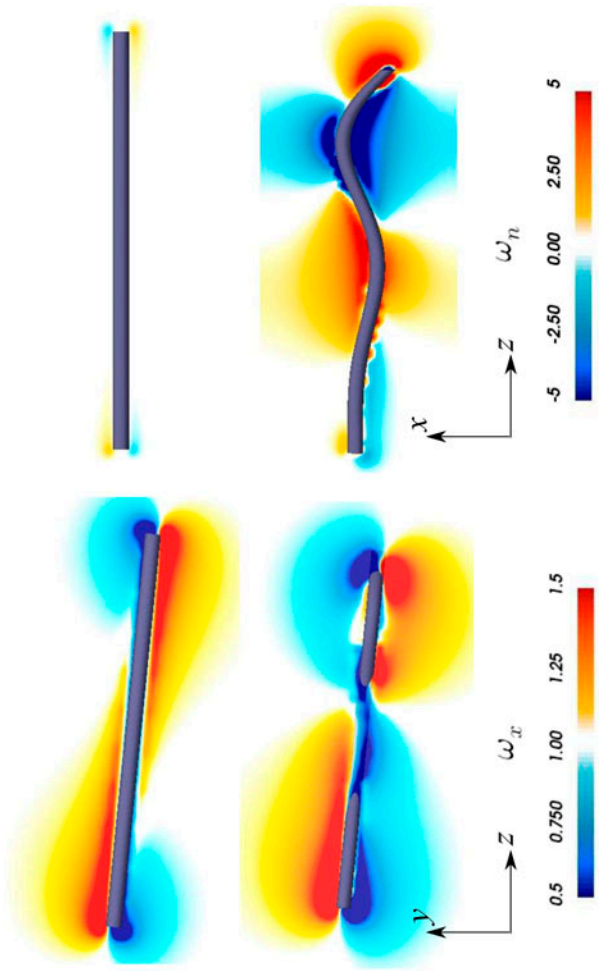
Figure 2. Visualisation of vorticity around the particles in two perpendicular planes.
Notes: In the left side of the figure, flow vorticity along the x-direction is shown for simulations of passive (upper part) and active (lower part) particles. In the right side of the figure, out-of-plane vorticity is shown in the mid-plane that passes through the body and perpendicular to the left plane.
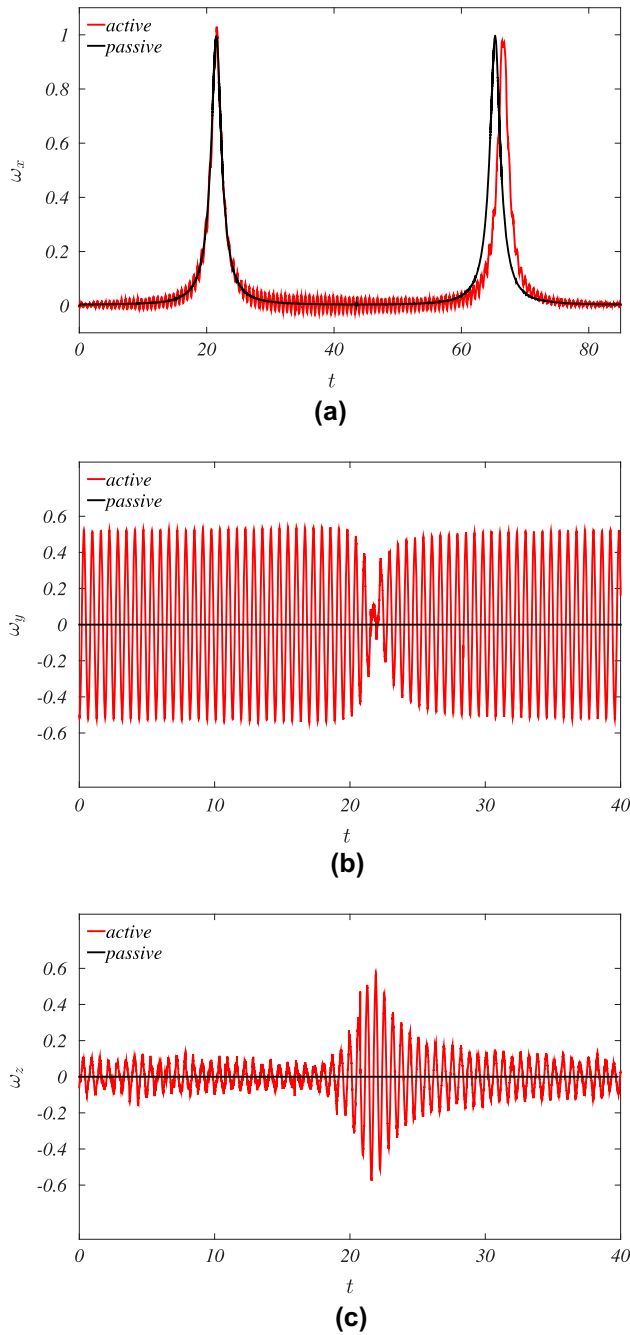
Figure 3. Instantaneous angular velocity of active and passive particles about (a) vorticity direction, (b) gradient direction, and (c) velocity direction.

Notes: For ω_x a whole cycle is shown, whereas for ω_y and ω_z only a half cycle is shown as they are symmetric for the other half.

both particles have very close average values of ω_x and period of rotation (see Table 1) and they spend most of their time aligned with the flow. Table 1 shows that the average angular velocity for both particles are about $\overline{\omega_x} \approx .07$, which

Table 1. Average angular velocity $\overline{\omega_x}$, period of rotation T, Average shear particle stress $\text{Sym}(\overline{\Sigma_{yz}^p})$, intrinsic viscosity $[\eta]$.

Case	$\overline{\omega_x}$	T	$\overline{\Sigma_{yz}^p}$	$[\eta]$
Active	.0685	90.1	.01074	9.70
Passive	.0721	87.2	.01064	9.61

is considerably lower than the bulk vorticity of flow. In fact, our results show at 80% of the rotation time both particles have angular velocity smaller than their average value.

Other components of angular velocity vector, ω_y and ω_z, are shown in Figure 3(b) and 3(c), respectively. We can clearly see that these components of angular velocity for an active particle have a cyclic behaviour similar to ω_x. The amplitude of these velocities is also comparable with ω_x, even though their cycle average is close to zero. Oscillations of ω_y and ω_z resembles a high-frequency kayaking motion of a spheroid(rod) in the shear flow (Tao, den Otter, & Briels, 2005). In this motion, which can be seen in rigid particles whose long axes initially make non-zero angles with the shear plane, a particle exhibits motions akin to that of the paddles of somebody kayaking (Tao et al., 2005). Comparing Figure 3(a)–3(c), one can see that when amplitude of ω_x reaches its maximum value ($t \approx 22$), amplitude of ω_y and ω_z are minimum and maximum, respectively. This is due to the effect of undulations on the exerted torque on the active particle. The total exerted torque on the particle is the result of the shear flow and body undulations. The shear flow generates a torque along the x-axis, whereas the torque due to body undulations is perpendicular to $X - Z$ plane (the plane in which the body undulates and rotate with shear flow), i.e. Y direction in Figure 1(b). At this time, the particle is oriented vertically with respect to inertial frame of reference and undulates in the $x - y$ plane, and consequently, generated torque due to undulations has a major component along the z-axis and almost no component along the y-axis. Therefore, the amplitude of angular velocity along z and y directions is maximum and minimum, respectively. ω_y and ω_z are calculated and found to be close to zero, i.e. negligible, for the passive particle. We conclude that the passive rod just simply tumbles (rotates) as it is initially aligned along the flow axis (very close to a rigid spheroid at the highest Jeffery's orbit Jeffery, 1922), whereas, the active rod not only tumbles, but also performs a high-frequency kayaking motion around its low-frequency rotational orbit.

3.2. Particle stress and intrinsic viscosity of the suspension

Shear particle stress Σ_{yz}^p is an important rheological parameter of a suspension, as it determines the relative viscosity of the suspension (η_r in Equation (11)). Figure 4 shows the instantaneous shear particle stress during particle's rotation for both simulations of active and passive particles. As expected, the particle stress is a periodic function of time with frequencies equal to that of the angular
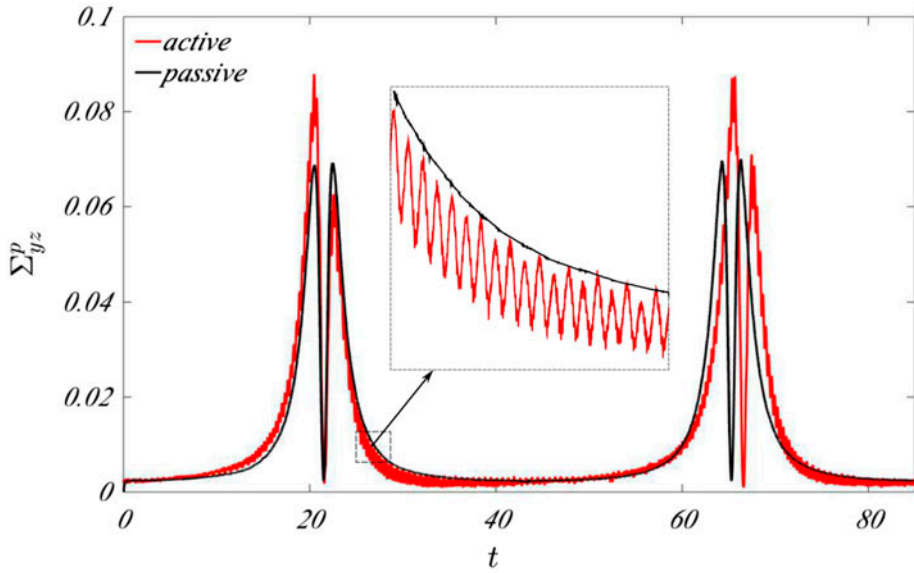
Figure 4. Instantaneous shear particle stress for active and passive rods.
Notes: Particle stress is a periodic function of time with frequencies equal to that of the angular velocity. Self-propulsion can slightly increase the shear particle stress and consequently intrinsic viscosity of a suspension.

velocity. The high-frequency oscillations can be observed by zooming around the plot of particle stress as shown by the inset in Figure 4.

Comparing particle stress in this figure with the angular velocity ω_x in Figure 3(a), the highest amplitude of particle stress associated with the highest amplitude of ω_x, i.e. particles have the highest projected area against the flow. This figure clearly shows that shear particle stress of both cases are very close and active particle has a relatively high value around peaks, but this difference is not very influential when average values are taken into account (either time-average or cycle-average) as can be seen in Table 1. For dilute suspensions of microswimmers, effective viscosity is typically studied by considering intrinsic viscosity $[\eta] = (\eta_r - 1)\phi^{-1}$ (Haines et al., 2009). This constant for non-Brownian suspensions depends on the shape, size and orientation of particles and can be determined analytically for simple shapes in dilute regimes (Jeffery, 1922; Leal & Hinch, 1971) and experimentally for more complicated geometries and high concentrations (Jeffrey & Acrivos, 1976; Mueller, Llewellin, & Mader, 2010). The value of intrinsic viscosity (based on the average value of shear particle stress) is calculated here and found to be $[\eta] = 9.61$ for the passive rod and $[\eta] = 9.70$ for the active one, which does not show a meaningful difference due to self-propulsion.

Modelling a bacterium as a rigid prolate spheroid in a Stokesian fluid, Haines et al. (2009) obtained the particle stress analytically as a function of particle's shape and orientation and addressed a decrease in the intrinsic viscosity due to self-propulsion. However, as can be qualitatively seen in Figure 4(a), this is not the

case in our simulations, i.e. self-propulsion has not changed the intrinsic viscosity of the suspension. To explain this contradiction, some of their implemented assumptions and ours need to be discussed. The decrease in viscosity is apparent only in weak shear and for strong shear (our simulations are at relatively high shear rate of $\dot{\gamma} = 1.0$) the effect of self-propulsion becomes negligible. Another important assumption is that the reduction in viscosity in their model relies on the swimmer being a 'pusher' and for a 'puller' swimmer self-propulsion cause an increase in viscosity. It should be noted that being a pusher and puller is based on a model for a spherical microswimmer (squimer) in Stokes flow, i.e. no inertia. Our swimming rod can be considered a pusher. However, the inertia in our simulations cannot be ignored (Re = 1.0), i.e. the inertia might be another source of this discrepancy.

4. Conclusion

We investigated the role of self-propulsion on the motion of a moderate aspect ratio rod in a shear flow and its effect on the viscosity of the suspension at very dilute concentration $\phi = .001$. The active particle moves through a shear flow by passing a travelling wave and at the same time rotates due to the exerted hydrodynamical torque from the background shear flow. In comparison with a rigid rod in a passive suspension, an undulatory rod revealed a more complicated kinematics and the angular velocity consists of oscillations with two frequencies, a higher frequency equal to the body undulation frequency and a lower one due to the external shear flow. The body motion also causes a high-frequency kayaking motion in the orbit of rotation for the active particle. We found that self-propulsion does not make a fundamental difference in the time period of rotation and the average value of angular velocity. We also calculated and compared the particle stress and intrinsic viscosity of the suspension for both cases (active and passive suspensions) and found that self-propulsion did not significantly change these values, which is in contrast with some previous studies that indicate the opposite role (significant reduction) for self-propelling particles in a dilute suspension probably due to high shear rate and inertia (Re = 1.0) of our simulations.

It should be noted that our results and conclusion are based on one case with (single values of shear rate and Reynolds number). We plan to perform simulations over a range of shear rate and Reynolds number to study the effects of these parameters on particle stress and intrinsic viscosity of a suspension.

Disclosure statement

Funding

ORCID

Iman Borazjani 🔴 http://orcid.org/0000-0001-7940-3168

References

Aidun, C. K., & Clausen, J. R. (2010). Lattice-boltzmann method for complex flows. *Annual Review of Fluid Mechanics, 42*, 439–472.

Asgharzadeh, H., & Borazjani, I. (2016). A newton–krylov method with an approximate analytical jacobian for implicit solution of navier–stokes equations on staggered overset-curvilinear grids with immersed boundaries. *Journal of Computational Physics. 331*, 227–256. doi: 10.1016/j.jcp.2016.11.033

Asgharzadeh, H., & Borazjani, I. (2016). Effects of reynolds and womersley numbers on the hemodynamics of intracranial aneurysms. *Computational and Mathematical Methods in Medicine, 2016*, 7412926. doi: 10.1155/2016/7412926

Balasubramanian, S., Kagan, D., Jack Hu, C.-M., Campuzano, S., Lobo-Casta non, M. J., Lim, N., ... Wang, J. (2011). Micromachine-enabled capture and isolation of cancer cells in complex media. *Angewandte Chemie International Edition, 50*, 4161–4164.

Balay, S., Buschelman, K., Gropp, W. D., Kaushik, D., Knepley, M. G., McInnes, L. C., & Zhang, H. (2001). PETSc Web page. http://www.mcs.anl.gov/petsc.

Baraff, D. (2001). An introduction to physically based modeling: Rigid body simulation I – Unconstrained rigid body dynamics. *SIGGRAPH Course Notes*, *2*, G1–68. Retrieved from http://graphics.cs.cmu.edu/courses/15-869-F08/lec/14/notesg.pdf

Batchelor, G. K. (1970). The stress system in a suspension of force-free particles. *Journal of Fluid Mechanics, 41*, 545–570.

Becker, A. D., Masoud, H., Newbolt, J. W., Shelley, M., & Ristroph, L. (2015). Hydrodynamic schooling of flapping swimmers. *Nature Communications, 6*.

Borazjani, I., Ge, L., & Sotiropoulos, F. (2008). Curvilinear immersed boundary method for simulating fluid structure interaction with complex 3d rigid bodies. *Journal of Computational Physics, 227*, 7587–7620.

Brennen, C., & Winet, H. (1977). Fluid mechanics of propulsion by cilia and flagella. *Annual Review of Fluid Mechanics, 9*, 339–398.

Daghooghi, M., & Borazjani, I. (2014, August 17–20). Parallel implementation of periodic boundary conditions for a curvilinear immersed boundary method. In *ASME 2014 International Design Engineering Technical Conferences and Computers and Information in Engineering Conference*, Volume 1A: 34th Computers and Information in Engineering Conference. (pp. V01AT02A019–V01AT02A019), New York, USA. American Society of Mechanical Engineers.

Daghooghi, M., & Borazjani, I. (2015). The influence of inertia on the rheology of a periodic suspension of neutrally buoyant rigid ellipsoids. *Journal of Fluid Mechanics, 781*, 506–549.

Daghooghi, M., & Borazjani, I. (2015). The hydrodynamic advantages of synchronized swimming in a rectangular pattern. *Bioinspiration & Biomimetics, 10*, 056018.

Daghooghi, M., & Borazjani, I. (2016). Self-propelled swimming simulations of bio-inspired smart structures. *Bioinspiration & Biomimetics, 11*, 056001.

Elgeti, J., Winkler, R. G., & Gompper, G. (2015). Physics of microswimmers – Single particle motion and collective behavior: A review. *Reports on Progress in Physics, 78*, 056601.

Gazzola, M., Tchieu, A. A., Alexeev, D., de Brauer, A., & Koumoutsakos, P. (2016). Learning to school in the presence of hydrodynamic interactions. *Journal of Fluid Mechanics, 789*, 726–749.

Ge, L., & Sotiropoulos, F. (2007). A numerical method for solving the 3d unsteady incompressible navier-stokes equations in curvilinear domains with complex immersed boundaries. *Journal of Computational Physics, 225*, 1782–1809.

Gilmanov, A., & Sotiropoulos, F. (2005). A hybrid cartesian/immersed boundary method for simulating flows with 3d, geometrically complex, moving bodies. *Journal of Computational Physics, 207*, 457–492.

Gyrya, V., Lipnikov, K., Aranson, I. S., & Berlyand, L. (2011). Effective shear viscosity and dynamics of suspensions of micro-swimmers from small to moderate concentrations. *Journal of Mathematical Biology, 62*, 707–740.

Haddadi, H., & Morris, J. (2014). Microstructure and rheology of finite inertia neutrally buoyant suspensions. *Journal of Fluid Mechanics*, *749*, 431–459. doi:10.1017/jfm.2014.238

Haines, B. M., Sokolov, A., Aranson, I. S., Berlyand, L., & Karpeev, D. A. (2009). Three-dimensional model for the effective viscosity of bacterial suspensions. *Physical Review E, 80*, 041922.

Hatwalne, Y., Ramaswamy, S., Rao, M., & Simha, R. A. (2004). Rheology of active-particle suspensions. *Physical Review Letters, 92*, 118101.

Jeffery, G. B. (1922). The motion of ellipsoidal particles immersed in a viscous fluid. *Proceedings of the Royal Society of London A: Mathematical, Physical and Engineering Sciences, 102*, 161–179.

Jeffrey, D. J., & Acrivos, A. (1976). The rheological properties of suspensions of rigid particles. *AIChE Journal, 22*, 417–432.

Lauga, E., & Powers, T. R. (2009). The hydrodynamics of swimming microorganisms. *Reports on Progress in Physics, 72*, 096601.

Leal, L. G., & Hinch, E. J. (1971). The effect of weak brownian rotations on particles in shear flow. *Journal of Fluid Mechanics, 46*, 685–703.

Li, G., Müller, U. K., van Leeuwen, J. L., & Liu, H. (2012). Body dynamics and hydrodynamics of swimming fish larvae: A computational study. *Journal of Experimental Biology, 215*, 4015–4033.

Mueller, S., Llewellin, E. W., & Mader, H. M. (2010). The rheology of suspensions of solid particles. *Proceedings of the Royal Society A: Mathematical, Physical and Engineering Science, 466*, 1201–1228.

Ozin, G. A., Manners, I., Fournier-Bidoz, S., & Arsenault, A. (2005). Dream nanomachines. *Advanced Materials, 17*, 3011–3018.

Rosén, T., Do-Quang, M., Aidun, C. K., & Lundell, F. (2015). The dynamical states of a prolate spheroidal particle suspended in shear flow as a consequence of particle and fluid inertia. *Journal of Fluid Mechanics, 771*, 115–158.

Saintillan, D., & Shelley, M. J. (2007). Orientational order and instabilities in suspensions of self-locomoting rods. *Physical Review Letters, 99*, 058102.

Saintillan, D., & Shelley, M. J. (2015). Theory of active suspensions. In S. E. Spagnolie (Ed.), *Complex fluids in biological systems* (pp. 319–355). New York, NY: Springer.

Sokolov, A., & Aranson, I. S. (2009). Reduction of viscosity in suspension of swimming bacteria. *Physical Review Letters, 103*, 148101.

Sokolov, A., Aranson, I. S., Kessler, J. O., & Goldstein, R. E. (2007). Concentration dependence of the collective dynamics of swimming bacteria. *Physical Review Letters, 98*, 158102.

Tao, Y.-G., den Otter, W. K., & Briels, W. J. (2005). Kayaking and wagging of rods in shear flow. *Physical Review Letters, 95*, 237802.

Toner, J., Tu, Y., & Ramaswamy, S. (2005). Hydrodynamics and phases of flocks. *Annals of Physics, 318*, 170–244.

Wensink, H. H., & Löwen, H., (2012). Emergent states in dense systems of active rods: From swarming to turbulence. *Journal of Physics: Condensed Matter, 24*, 464130.

Willert, C. E., & Gharib, M. (1991). Digital particle image velocimetry. *Experiments in Fluids, 10*, 181–193.

Yang, Y., Marceau, V., & Gompper, G. (2010). Swarm behavior of self-propelled rods and swimming flagella. *Physical Review E, 82*, 031904.